Journal of Alloys and Compounds 509 (2011) 764–768

Contents lists available at ScienceDirect

Journal of Alloys and Compounds

journal homepage: www.elsevier.com/locate/jallcom

A novel Bi-based oxychloride $CdBiO_2Cl$: Crystal structure, electronic structure and photocatalytic activity

Fuqiang Huang*, Jianjun Wu, Xinping Lin, Zhen Zhou**

CAS Key Laboratory of Materials for Energy Conversion, Shanghai Institute of Ceramics, Chinese Academy of Sciences (SICCAS), Shanghai, PR China

ARTICLE INFO

Article history:
Received 9 April 2010
Received in revised form
10 September 2010
Accepted 18 September 2010
Available online 25 September 2010

Keywords:
Layered structure
Photocatalysis
Ag-loading
Bi-based
Electronic structure

ABSTRACT

$CdBiO_2Cl$ with layered structure as a novel efficient photocatalyst was synthesized by a solid state reaction method. The optical band gap of $CdBiO_2Cl$ is determined to be 3.08 eV by UV–vis diffuse reflectance spectroscopy. The photocatalytic activity of $CdBiO_2Cl$ for degrading methyl orange (MO) is much higher than that of commercially obtained anatase TiO_2 under UV light illumination. The Ag-loading over $CdBiO_2Cl$ leads to an obvious increase in the photocatalytic performance. The photocatalytic activity is discussed in close connection with the crystal structure and the electronic structure.

1. Introduction

As a potential solution to the severe problems of energy shortages and environment crises, photocatalysis has attracted ever-increasing attention for a great deal of advantages such as unlimited resources, low cost, and environmental friendliness. The general photocatalytic process of a semiconductor involves the formation of photoinduced electrons at the conduction band and holes at the valence band, and subsequent chemical reactions with the surrounding media after the photoinduced charges move to powder surface. In this way, water can be split into H_2 and O_2, and pollutants in water or gas can be effectively degraded or purified.

During the last two decades, besides the focused work on TiO_2 modifications, many efforts were made to develop other novel efficient photocatalysts. The reported photocatalyst systems, to the best of our knowledge, can be generally classified as oxides [1–8], sulfides [9–11], oxysulfides [12], nitrides [13–16], and oxynitrides [17,18]. Recently, Bi-based oxychlorides have drawn our attentions for their potential application as novel photocatalysts owing to their unique layered structures and high chemical stabilities [19–24]. The Bi-based oxychloride is the Sillén family expressed by $[M_2O_2][Cl_m]$ (m = 1–3) [19–21], where bismuth oxide-based fluorite-like layers, $[M_2O_2]$, are intergrown with single, double, or triple chlorine layers to construct such compositions as $CdBiO_2Cl$, BiOCl, etc. The extending Bi-based oxychlorides are the Sillén–Aurivillius intergrows $[Bi_2O_2][A_{n-1}B_nO_{3n+1}][Bi_2O_2][Cl_m]$ [22–24], where the Aurivillius family $[Bi_2O_2][A_{n-1}B_nO_{3n+1}]$ is intergrown with the structure-similarity Sillén family $[Bi_2O_2][Cl_m]$, i.e., Bi_4TaO_8Cl, Bi_4NbO_8Cl, etc. Besides the unique layer structure, a hybrid state in the conduction band (CB) and/or valence band (VB) will predict additional promotion of the photocatalysis efficiency due to the fair mobility of photogenerated charges resulted from the large dispersion [25,26]. Intrigued by the synergistic effects of layer structure and band dispersion, it is of great interest and importance to develop layered oxychloride with hybridized energy band for photocatalysis application.

In this paper, we proved the feasibility to use the Bi-based oxychloride $CdBiO_2Cl$ as an efficient photocatalyst for degrading methyl orange (MO). More importantly, combined with the intrinsic layer structure and the highly dispersed states in the CB and VB, the photocatalytic activity of $CdBiO_2Cl$ is much higher than that of commercially used anatase TiO_2 under UV light illumination. The successful confirmation of the high photocatalytic activity of $CdBiO_2Cl$ here may imply a series of stable Bi-based oxychlorides as candidates for high performance photocatalysts.

2. Experimental

2.1. Synthesis of the sample

The $CdBiO_2Cl$ powders were synthesized by a solid state reaction method. The well-mixed starting materials of BiOCl [27] and CdO (AR, 99.5%) with the stoichiometric proportion were firstly calcined at 700 °C for 2 h in an alumina crucible in

* Corresponding author. Tel.: +86 21 52411620; fax: +86 21 52416360.
** Corresponding author. Fax: +86 21 52416360.
E-mail addresses: huangfq@mail.sic.ac.cn (F. Huang), zhenzhou2009@gmail.com (Z. Zhou).

0925-8388/$ – see front matter © 2010 Elsevier B.V. All rights reserved.
doi:10.1016/j.jallcom.2010.09.081

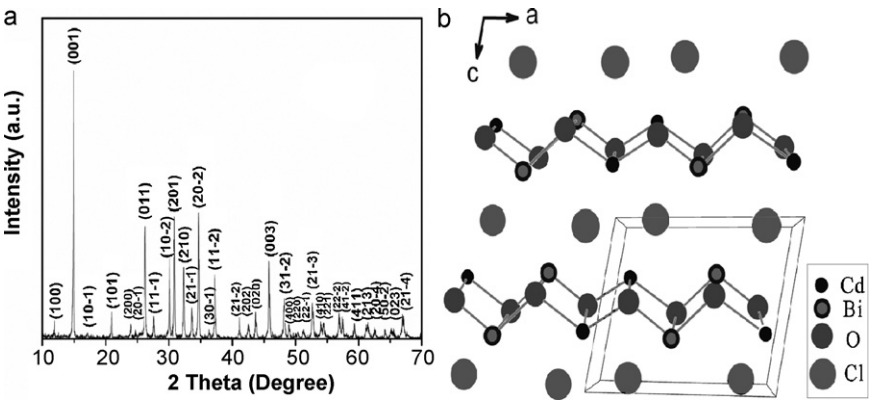

Fig. 1. (a) X-ray diffraction pattern and the layered structure of $CdBiO_2Cl$.

air. After a 15-min grinding, the sample was re-heated at 700 °C for 22 h. The formation of the oxychloride was confirmed by X-ray diffraction (XRD) analysis. The optical band gap was estimated from the UV–vis diffuse reflectance spectrum. In order to increase the photocatalytic efficiency, silver metal was loaded on the surface of $CdBiO_2Cl$ by a wet chemical reduction method under UV irradiation for 4 h, using $AgNO_3$ as Ag source and methanol to capture photoinduced-holes, followed by being dried at 353 K for 5 h in air.

2.2. Photocatalytic tests

The photocatalytic reactor consists of two parts, a quartz cell with a circulating water jacket and a 300 W high-pressure mercury lamp with a maximum emission at 365 nm placed inside the quartz cell. The volume of the initial 10 mg/L MO solution is 300 mL. In all experiments, the reaction temperature was kept at room temperature to prevent any thermal catalytic effect using the circulating water jack. The powder concentration in the neutral MO aqueous solution (pH = 6.93) ranges from 0.1 g/100 mL to 0.3 g/100 mL. UV illumination was conducted after the suspension was magnetically stirred in the dark for 50 min to reach the adsorption–desorption equilibrium of MO on catalysts. During irradiation, about 3 mL suspension was continually taken from the reaction cell at given time intervals for subsequent MO concentration analysis after centrifuging.

3. Results and discussion

3.1. Crystal structure and optical properties

The $CdBiO_2Cl$ powders were synthesized by a solid state reaction method, using BiOCl [21] and CdO as starting materials. The phase is confirmed by XRD analysis as shown in Fig. 1a, and all the peaks are indexed according to the standard JCPDS 51-0267. $CdBiO_2Cl$ crystallizes in the P21/m space group with the monoclinic crystal structure, as shown in Fig. 1b. The structure shows a layered configuration [28]. The [$CdBiO_2$] and [Cl] slices are one by one orderly piled up along the *c* axis to form the unique layered structure. It is believed that the permanent electric fields between [$CdBiO_2$] and [Cl] slabs can work as accelerators for the separations of electron–hole pairs upon photoexcitation, facilitating the high photocatalytic efficiency of $CdBiO_2Cl$. The Bi^{3+} and Cd^{2+} are in a similar coordination environment. Four oxygen ions and three chlorine ions are coordinated to a Bi ion. The Bi–O bond distances in the BiO_4Cl_3 local structure range from 2.1596 Å to 2.2978 Å, while the Bi–Cl bond distances are longer from 3.3201 Å to 3.4083 Å. Such long Bi–Cl bonds commonly exist in the oxychlorides, for example, 3.146–3.474 Å in $Bi_{12}O_{15}Cl_{16}$, 3.224–3.314 Å in Bi_3O_4Cl, and 3.059 Å in BiOCl. It is attributed to the stereochemically active Bi $6s^2$ lone electron pairs. As stated above, the Cd^{2+} ion is sited at a spatial position similar to Bi^{3+}, thus, it also has a seven-coordination environment, with four Cd–O bond distances from 2.2010 Å to 2.4531 Å, one Cd–Cl bond distance at 2.4877 Å and another two Cd–Cl bond distances at the same value of 3.3483 Å. Generally, the BiO_4Cl_3 polyhedron is relatively geometrically irregular owing to the presence of Bi $6s^2$, as compared to CdO_4Cl_3.

Fig. 2 shows the UV–vis diffuse reflectance spectrum of $CdBiO_2Cl$. It can be seen that the light absorption starts at about 450 nm, and the absorbance sharply increases below about 400 nm. The optical band gap was determined by the following equation using the data of optical absorption vs. wavelength near the band edge [29,30], $\alpha h\nu = A(h\nu - E_g)^{n/2}$, where α, ν, A, E_g are absorption coefficient, light frequency, proportionality constant, and band gap, respectively. In the equation, n decides the characteristics of the transition in a semiconductor, i.e., a direct transition for $n = 1$ and an indirect transition for $n = 4$. The value of n and E_g was determined by the following steps: first, plot $\ln(\alpha h\nu)$ vs. $\ln(h\nu - E_g)$, using an approximate value of E_g, and then determine the value of n with the slope of the straight line near the band edge; second, plot $(\alpha h\nu)^{2/n}$ vs. $h\nu$ and then evaluate the band gap E_g by extrapolating the straight line to the $h\nu$ axis intercept. By this means, the value of n for the present compound was determined at 4. This shows that the optical transitions for the oxychloride are indirectly allowed, which is in good agreement with the result of below-discussed band structure that $CdBiO_2Cl$ is a direct gap material while the indirect electron transitions are strongly allowed, and its band gap was estimated at 3.08 eV.

3.2. Electronic structure

Electronic structure of $CdBiO_2Cl$ was calculated by TB-LMTO program, which is a self-consistent, scalar relativistic linearized muffin-tin orbital program by Andersen and co-workers within the atomic sphere approximation [31–33]. This method splits the crystal space into overlapping atomic spheres (Wigner–Seitz spheres)

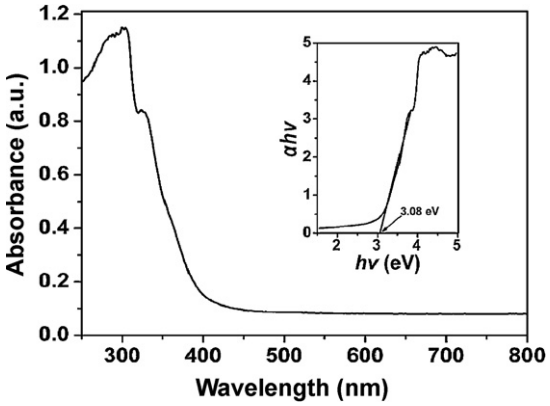

Fig. 2. UV–vis diffuse reflectance spectrum of $CdBiO_2Cl$.

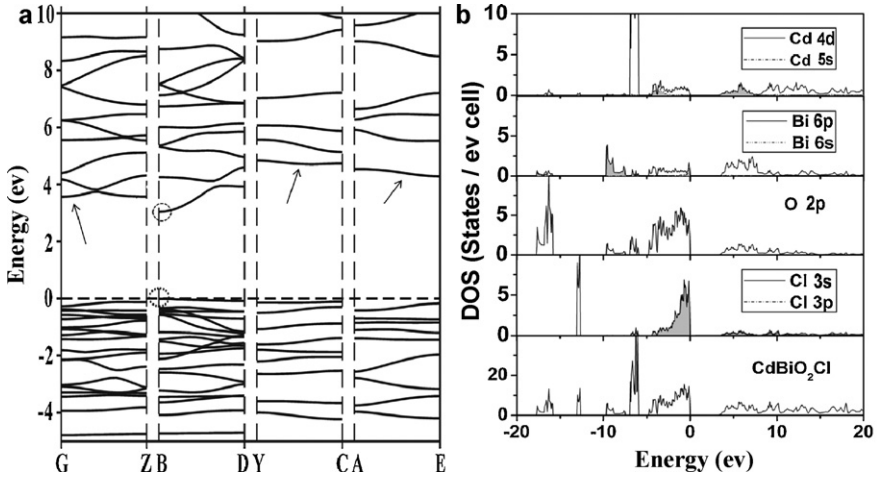

Fig. 3. (a) Band structure, (b) partial and total density of state (DOS) of $CdBiO_2Cl$.

whose radii are chosen to fill completely the crystal volume. In the present calculations, the von Barth–Hedin exchange-correlation potential was used within the local density approximation (LDA) [34]. All *k*-space integrations were performed with the tetrahedron method [35–36]. The basis sets consisted of the valence 4d, 5s and 5p states for Cd, 6s and 6p states for Bi, 2s and 2p states for O, 3s and 3p states for Cl and 1s for empty spheres. The 6d states for Bi, 3d states for O and Cl, and p–d states for empty spheres were downfolded by means of the technique described by Löwdin [37]. Within the Brillouin zone of the cell, 238 irreducible *k*-points from 768 were used. The high-symmetry points are G (0, 0, 0), Z (0, 0, 1/2), B (−1/2, 0, 0), D (−3/8, 0, 1/2), Y (0, 1/2, 0), C (0, 1/2, 1/2), A (−1/2, 1/2, 0), and E (−3/8, 1/2, 1/2) in terms of the reciprocal basis vectors [38].

The band structure of $CdBiO_2Cl$ is displayed in Fig. 3a. The lowest unoccupied state and the highest occupied state are both at the B point. This means $CdBiO_2Cl$ a direct gap material. The calculated gap (3.05 eV) is rather consistent with the measured optical band gap (3.08 eV). There are two bands in the region from 3.05 eV to 5.0 eV above the Fermi level, Bi 6p and Cd 5s orbitals, respectively. The bands just below the Fermi level are composed of Cl 3p and O 2p orbitals, hybridized by Bi 6s and Cd 4d orbitals, as shown in Fig. 3b. In other words, the conduction band minimum (CBM) is composed of Bi 6p and Cd 5s orbitals; the valence band maximum (VBM) primarily consists of Cl 3p and O 2p orbitals, hybridized by Bi 6s and Cd 4d orbitals. Notice that the dispersion in the Cd 5s bands is very large in the conduction band. The large dispersion in the band structure corresponds to small density states, and small dispersion (flat bands) corresponds to large density states. Therefore, the direct transition at B point is rather weak. The strong optical transitions are due to flat bands from the valence band to the conduction band. Flat curves in the valence band are found along G point to Z point, Y point to C point and A point to E point, among which the GZ curve is at a lowest energy level. In the same way, the flat curve with a highest energy level in the conduction band is around the point B. The indirect transition from highest occupied states at a flat curve in the valence band to the unoccupied states at a flat curve in the conduction band, between B and Z (dashed circles in Fig. 4), exhibits a gap about 3.71 eV and the corresponding strong absorption of 334 nm, which is in good agreement with the inflexion point at about 326 nm in the UV–vis diffuse reflectance spectrum in Fig. 2. The strong dispersion of the S-type conduction band commonly observed for most transparent conducting oxides (TCOs) gives rise to an excellent transport and conducting properties. This has been observed in CdO, In_2O_3, ZnO, Cd_2SnO_4 and SnO_2. For example, the commercial Sn doped In_2O_3 (ITO), the most famous n-type TCO, has the carrier concentration of 10^{20} to 10^{21} cm^{-3}, the resistivity of 10^{-4} ohm cm and the carrier mobility of 30 cm^2 v^{-1} s^{-1}. Such excellent electron conducting properties of TCOs can be ascribed to the large dispersion of outer ns orbitals. As mentioned above, $CdBiO_2Cl$ has also the strong dispersion of the S-type conduction band, just like most n-type TCOs. Therefore, the Cd 5s states of $CdBiO_2Cl$ are expected to be a good media to transport the electrons. Additionally, the hybrid states that can lead to the fair dispersions in the conduction and valence bands in $CdBiO_2Cl$ may also imply a fair mobility of photogenerated charges to travel a long

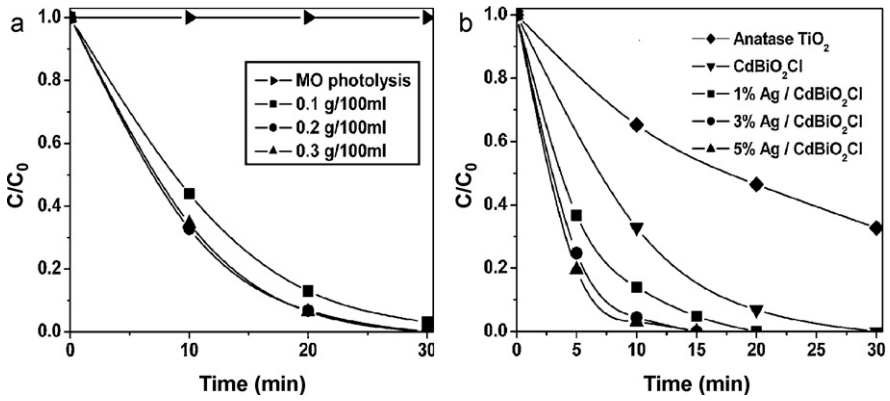

Fig. 4. (a) Effect of the catalyst concentration on the photocatalytic efficiency, (b) photocatalytic activities of TiO_2, $CdBiO_2Cl$ and Ag-loaded $CdBiO_2Cl$.

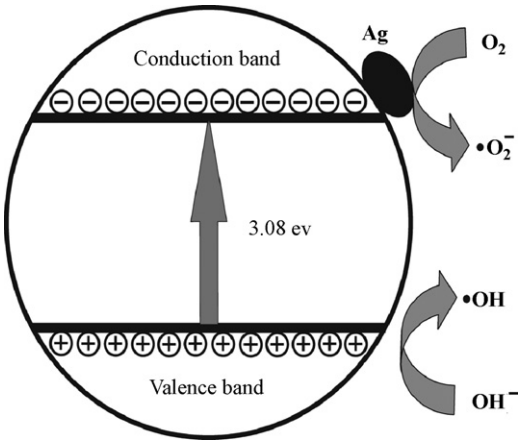

Fig. 5. The proposed mechanism of the improvement of photocatalytic activity by Ag loading.

distance, assisting the photo-stimulated electron–hole separations and improving the photocatalytic activity of the compound.

3.3. Photocatalytic activity

3.3.1. Effect of the catalyst concentration in suspensions

Fig. 4a shows the effects of the $CdBiO_2Cl$ concentration on the MO decomposition ratio. The percentage of decomposition higher than 97% over the photocatalyst with three different concentrations can be achieved as the irradiation time comes to 30 min. The MO degradation by the photolysis in the blank experiment is negligible and the photocatalytic efficiencies with the catalyst concentrations of 0.2 g/100 mL and 0.3 g/100 mL are almost the same, both higher than that with the concentration of 0.1 g/100 mL. The above slight difference of the catalytic efficacies results from the competition between the larger photocatalytically activated surface and the stronger light reflection on the photocatalyst powder as the concentration increases from 0.2 g/100 mL to 0.3 g/100 mL.

3.3.2. The effect of Ag-loading

The MO photo-decolorization over TiO_2, $CdBiO_2Cl$ and Ag loaded $CdBiO_2Cl$ as a function of UV-irradiation time is presented in Fig. 4b. The concentrations of different powders in MO aqueous solutions are all 0.2 g/100 mL. The equilibrium adsorptions of MO on $CdBiO_2Cl$ and TiO_2 are 2.9% and 3.7% before the photocatalytic reactions. The slight difference of the two initial equilibrium adsorptions is believed not to affect the subsequent comparative discussion on the discrepancy of photocatalytic efficiencies over the two materials. It can be seen that the pure $CdBiO_2Cl$ exhibits a much higher photocatalytic activity compared to TiO_2, e.g., the MO removal over $CdBiO_2Cl$ at $t = 30$ min is 100% while only 67.3% over TiO_2. The Ag dispersion over $CdBiO_2Cl$ results in an obvious enhancement in the photocatalytic activity. The required time for an entire MO degradation decreases from 30 min to 15 min as the Ag loading mass increases from 0% to 5%. It is well-known that the Ag/semiconductor composite leads to the formation of a Schottky barrier [39–42]. Thus, the photoinduced electrons in the conduction band of the semiconductor are believed to readily transfer to Ag, which facilitates the separation of the photogenerated electron–hole pair and thus improves the photocatalytic activity. In this way, a larger amount of $\bullet O_2^-$ and •OH active oxidants that can degrade MO to intermediates and the final CO_2, are formed over the catalyst surfaces, enhancing the photocatalytic efficiencies (see Fig. 5).

4. Conclusions

A Bi-based oxychloride $CdBiO_2Cl$ with a layered structure was synthesized by a solid state reaction method. The conduction band minimum (CBM) is mainly composed of Bi 6p and Cd 5s orbitals, and the valence band maximum (VBM) primarily consists of Cl 3p and O 2p orbitals, hybridized by Bi 6s and Cd 4d orbitals. After equipped with, the internal electric fields resulted from $[CdBiO_2]$ and [Cl] slabs, and the highly dispersed states in the CB and VB caused by the hybridization of orbitals, the novel layered $CdBiO_2Cl$ exhibits much higher photocatalytic performance in comparison to the commercially obtained anatase TiO_2 under UV light illumination, especially with silver loading on its surface. This study discloses insights for the designed strategy of efficient photocatalysts with combined and synergistic features and sheds some light on the deliberate synthesis of other oxychloride functional materials.

Acknowledgements

Financial support from National 973 Program of China Grants (2007CB936704 and 2009CB939903), National Science Foundation of China Grants (50772123, 20901083 and 50902143), and Science and Technology Commission of Shanghai Grants (08JC1420200 and 0952nm06500) are gratefully acknowledged.

References

[1] Y.F. Tu, S.Y. Huang, J.P. Sang, X.W. Zou, J. Alloys Compd. 482 (2009) 382–387.
[2] Y.Y. Zhang, X.Y. Ma, P.L. Chen, D.R. Yang, J. Alloys Compd. 480 (2009) 938–941.
[3] M. Li, Z.L. Hong, Y.N. Fang, F.Q. Huang, Mater. Res. Bull. 43 (2008) 2179–2186.
[4] F. Lin, D.M. Jiang, X.M. Ma, J. Alloys Compd. 470 (2009) 375–378.
[5] J.J. Wu, X.J. Lü, F.Q. Huang, F.F. Xu, Eur. J. Inorg. Chem. 19 (2009) 2789–2795.
[6] J.J. Wu, X.J. Lü, F.Q. Huang, F.F. Xu, J. Alloys Compd. 496 (2010) 234–240.
[7] J.J. Wu, J.T. Li, F.Q. Huang, F.F. Xu, J. Mater. Chem. 20 (2010) 1942–1946.
[8] A.P. Zhang, J.Z. Zhang, J. Alloys Compd. 491 (2010) 631–635.
[9] T. Hirai, K. Suzuki, I. Komasawa, J. Colloid Interface Sci. 244 (2001) 262–265.
[10] M. Esmaili, A.H. Yangjeh, J. Alloys Compd. 496 (2010) 650–655.
[11] S.N. Zu, Z.Y. Wang, X.P. Fan, J. Alloys Compd. 476 (2009) 689–692.
[12] A. Ishikawa, T. Takata, J.N. Kondo, M. Hara, K. Domen, J. Phys. Chem. B 108 (2004) 2637–2642.
[13] W.J. Chun, J.N. Kondo, Y. Matsumoto, K. Domen, J. Phys. Chem. B 107 (2003) 1798–1803.
[14] M. Hara, G. Hitoki, T. Takata, H. Kobayashi, K. Domen, Catal. Today 78 (2003) 555–560.
[15] J. Sato, N. Saito, M. Hara, K. Domen, Y. Inoue, J. Am. Chem. Soc. 127 (2005) 4150–4151.
[16] S.S. Kocha, J.M. Redwing, M.A. Tischler, J.A. Turner, J. Electrochem. Soc. 142 (1995) L238.
[17] F. Chevire, F. Tessier, R. Marchand, Eur. J. Inorg. Chem. 6 (2006) 1223–1230.
[18] K. Maeda, D. Lu, T. Takata, N. Saito, Y. Inoue, K. Domen, Nature 440 (2006) 295–1295.
[19] V.A. Dolgikh, L.N. Kholodkovskaya, Russ. J. Inorg. Chem. 37 (1992) 488–501.
[20] S.M. Fray, C.J. Milne, P. Lightfoot, J. Solid State Chem. 128 (1997) 115–120.
[21] A.M. Kusainova, W. Zhou, J.T.S. Irvine, P. Lightfoot, J. Solid State Chem. 166 (2002) 148–157.
[22] D.O. Charkin, V.A. Dolgikh, P. Lightfoot, J. Solid State Chem. 175 (2003) 316–321.
[23] J.M. Thomas, W. Ueda, K.D.M. Harris, Faraday Discuss. Chem. Soc. 87 (1989) 33–37.
[24] R. Burch, S. Chalker, P. Loader, J.M. Thomas, W. Ueda, Appl. Catal. A 82 (1992) 77–81.
[25] J. Tang, Z. Zou, J. Ye, Angew. Chem. Int. Ed. 43 (2004) 4463–4466.
[26] X. Lin, Fu. Huang, W. Wang, Appl. Catal. A 307 (2006) 257–262.
[27] K.L. Zhang, F.Q. Huang, C. Zheng, Appl. Catal. B 68 (2006) 125–129.
[28] S.D. Kirik, E.G. Yakovleva, A.F. Shimanskii, Y.G. Kovalev, Acta. Crystallogr. C 57 (2001) 1367–1368.
[29] M.A. Butler, J. Appl. Phys. 48 (1977) 1914–1920.
[30] J. Tang, Z. Zou, J. Ye, J. Phys. Chem. B 107 (2003) 14265–14269.
[31] O.K. Andersen, Phys. Rev. B 12 (1975) 3060–3083.
[32] O.K. Andersen, O. Jepsen, Phys. Rev. Lett. 53 (1984) 2571–2574.
[33] O. Jepsen, O.K. Andersen, Z. Phys. B: Condens. Matter 97 (1995) 35–39.
[34] L. Hedin, B.I. Lundqvist, J. Phys. C: Solid State Phys. 4 (1971) 2064–2083.
[35] W.R.L. Lambrecht, O.K. Andersen, Phys. Rev. B 34 (1986) 2439–2449.
[36] O. Jepsen, O.K. Andersen, Solid State Commun. 9 (1971) 1763–1767.

[37] P.-O. LÖwdin, J. Chem. Phys. 19 (1951) 1396–1401.
[38] C.J. Bradley, A.P. Cracknell, The Mathematical Theory of Symmetry in Solids, Clarendon Press, Oxford, 1972.
[39] V. Subramanian, P.V. Kamat, J. Am. Chem. Soc. 126 (2004) 4943–4950.
[40] A.L. Linsebigler, G. Lu, J.T. Yates, Chem. Rev. 95 (1995) 735–758.
[41] Z. Shan, J. Wu, F. Xu, F. Huang, J. Phys. Chem. C 112 (2008) 15423–15428.
[42] T. Sano, N. Negishi, K. Uchino, K. Takeuchi, J. Photochem. Photobiol. A 160 (2003) 93–98.